J Mater Sci (2009) 44:2796–2804
DOI 10.1007/s10853-009-3368-0

Optical properties and microstructures of Pd-free Ag–Au–Pt–Cu dental alloys

Takanobu Shiraishi · Yasuko Takuma · Takeshi Fujita · Eri Miura · Kunihiro Hisatsune

Received: 6 August 2008 / Accepted: 23 February 2009 / Published online: 19 March 2009

Abstract Nine experimental Pd-free Ag–Au–Pt–Cu dental alloys containing 10 at.% Pt and 10–35 at.% Au were prepared and their optical properties and microstructures were investigated by means of spectrophotometric colorimetry, optical microscopy, and electron probe microanalysis. All the alloys were annealed at 850 °C and mirror-polished to observe their reflectance curves in the visible spectrum and three-dimensional color coordinates. All the alloys were composed of a major phase of Ag–Au-rich matrix and a minor and almost colorless Pt–Cu-rich phase. It was found that the color of the alloys was substantially controlled by the Ag–Au-rich matrix and that with increasing Au/Ag atomic ratio from 0.130 to 0.996, the yellow-blue chromaticity index b^* increased from 8.0 to 14.4, giving a pale yellow color. This systematic increase in yellowness was caused by a continuous shift of the absorption edge of reflectance curve toward longer wavelengths with increasing Au/Ag atomic ratio.

Introduction

Dental casting precious-metal alloys have been served for long periods as clinically reliable materials for crown and bridge restorations. Among them, the Au–Ag–Cu-based alloys usually contain a small amount of Pd and the Ag–Pd-based alloys may contain 25% Pd to prevent sulfurization of Ag in the oral environment [1]. However, the Pd price began to climb sharply in the late 1990s and peaked in the year 2000 and early 2001 [2]. This sharp rise in Pd price led to marked drops in Pd demand from the dental alloys market in the world [3]. In Europe, Pd-based dental alloys were widely substituted by alternatives, including ceramic products, following the spike in the price of Pd in 2000 and early 2001 [4]. Although the Pd price began to descend thereafter, it rose significantly again during the late 2005 and the first half of 2006 [5]. The significant rise and the subsequent slow drop of Pd price can lead to unstable supply of dental precious-metal alloys containing Pd.

Concerning the biological effects of Pd, Wataha and Hanks [6] reviewed the reported papers in response to the recent controversies over possible adverse biological effects of using Pd in dental alloys. They summarized that the risk of using Pd in dental casting alloys appears to be extremely low because of the low dissolution rate of Pd ions from these alloys [6]. However, they pointed out that Pd allergy almost always occurs in individuals who are sensitive to Ni [6]. Similarly, it was considered that if a patient is allergic to Ni, no Pd containing material should be incorporated [7].

Based on these backgrounds of the stable supply and the biological effects, we consider that the development of Pd-free dental casting precious-metal alloys and their stable supply to dental alloy market are meaningful and can contribute to the patients who are allergic or sensitive to Pd. Accordingly, we designed quaternary Ag–Au–Pt–Cu alloys containing 10 at.% Pt and 10–35 at.% Au as Pd-free low-gold dental casting alloys. Although the primary concerns about cast dental restorations are with biocompatibility and corrosion and tarnish resistance, it would be naive to discount the strong emotional attachment to

T. Shiraishi (✉) · Y. Takuma · T. Fujita · E. Miura · K. Hisatsune
Department of Dental and Biomedical Materials Science, Unit of Basic Medical Sciences, Graduate School of Biomedical Sciences, Nagasaki University, 1-7-1 Sakamoto, Nagasaki 852-8588, Japan
e-mail: siraisi@nagasaki-u.ac.jp

selected alloy colors involving Au [8]. This suggests that color control should be taken into account as one of the important criteria in designing dental precious-metal alloys containing Au. In fact, dental alloy manufacturers almost always indicate color of their gold alloy products. This may further demonstrate the importance of color control of dental precious-metal alloys containing Au.

In this research, variations of color with chemical composition in the experimental nine quaternary Ag–Au–Pt–Cu alloys for dental applications were investigated by means of spectrophotometric colorimetry, optical microscopy, and electron probe microanalysis. By analyzing the observed spectral reflectance curves, color coordinates and microstructures, trend in the shift of various colorimetric parameters with chemical composition was made clear.

Materials and methods

Sample preparation

Table 1 gives chemical compositions of the examined Ag–Au–Pt–Cu quaternary alloys. Numbers in parentheses indicate compositions of the prepared alloys determined by X-ray fluorescence analysis. In the present study, chemical compositions of the experimental alloys were designed on the atomic percentage basis. The concentration of Pt was fixed at 10 at.% for all the alloys and the concentration of Cu was fixed at either 10 at.% (alloys A, B, and C), 15 at.% (alloys D, E, and F), or 20 at.% (alloys G, H, and I). The concentration of Au was varied from 10 to 35 at.% with 5 at.% increments. As given in the right column of the Table 1, Au/Ag atomic ratio, calculated from the analyzed composition of the prepared alloys, widely varied from 0.130 for the alloy "A" to 0.996 for the alloy "I". For convenience, the analyzed compositions in mass % of the prepared alloys are given in Table 2.

Table 1 Chemical compositions of the Ag–Au–Pt–Cu quaternary alloys examined

Alloy	Composition (at. %)				Atomic ratio[a]
	Ag	Au	Pt	Cu	Au/Ag
A	70 (70.04)	10 (9.10)	10 (10.74)	10 (10.12)	0.130
B	60 (60.14)	20 (20.33)	10 (9.37)	10 (10.16)	0.338
C	50 (49.67)	30 (29.68)	10 (10.36)	10 (10.29)	0.598
D	60 (60.18)	15 (15.57)	10 (9.12)	15 (15.13)	0.259
E	50 (49.81)	25 (24.98)	10 (10.03)	15 (15.18)	0.502
F	40 (39.90)	35 (34.54)	10 (10.76)	15 (14.80)	0.866
G	55 (55.21)	15 (15.71)	10 (9.10)	20 (19.98)	0.285
H	45 (45.40)	25 (24.87)	10 (10.09)	20 (19.64)	0.548
I	35 (35.43)	35 (35.29)	10 (8.92)	20 (20.36)	0.996

Numbers in parentheses indicate the analyzed compositions of the prepared alloys

[a] Calculated from analyzed composition in parentheses

Table 2 Chemical compositions in mass % of the Ag–Au–Pt–Cu quaternary alloys examined (analyzed values)

Alloy	Composition (mass %)			
	Ag	Au	Pt	Cu
A	62.51	14.83	17.34	5.32
B	50.04	30.88	14.10	4.98
C	38.61	42.12	14.56	4.71
D	52.79	24.93	14.46	7.82
E	40.66	37.23	14.81	7.30
F	30.42	48.09	14.84	6.65
G	49.24	25.59	14.67	10.50
H	37.63	37.65	15.13	9.59
I	27.68	50.35	12.60	9.37

High purity component metals were used as starting materials. Appropriate amounts of component pure metals were accurately weighed and melted together under argon atmosphere in a high frequency induction furnace. Ingots obtained were subjected to alternate cold rolling and annealing heat treatment at high temperatures. A number of plate samples with size $10 \times 10 \times 0.5$ mm^3 were obtained and subjected to the following experiments.

Spectrophotometric colorimetry

Three plate samples from each alloy were annealed at 850 °C for 30 min in Ar gas stream and quenched into ice brine. They were individually embedded in cold-curing-type epoxy resin and subjected to the wet grinding process. The wet grinding of the samples was performed using a series of waterproof abrasive papers adhered to a turntable in an automatic polishing apparatus (MA-150, Musashino Denshi Co., Ltd., Tokyo, Japan). After being ground down to a 2000-grit finish, the samples were loaded on another automatic polishing apparatus (Doctor-Lap ML-180, Maruto Instrument Co., Ltd., Tokyo, Japan) and successively polished using a polishing cloth filled with aluminum oxide suspension with a grain diameter of 0.3 μm and 0.06 μm.

The polished samples were rinsed with pure water, dried, and then mounted on a computer-controlled spectrophotometer (CM-3600d, Konica Minolta Sensing, Inc., Osaka, Japan) with a dual-beam system. The EVER-WHITE (Code No. 9582, Evers Corporation, Osaka, Japan) plate with the traceability of National Physical Laboratory, UK, was used as a white reflection standard in the current study. The standard deviation for reflectance by 30 repeated measurements was certified to be less than 0.1%. Spectral reflectance data from the mirror-polished flat samples were recorded at

10 nm intervals from 360 to 740 nm with the geometry of diffuse illumination and 8° viewing. Because of the high reflective nature of the sample, the specular-component-included configuration was employed in the spectral reflectance measurements. Three-dimensional color coordinates, i.e., L^*_{ab} (lightness), a^* (red-green chromaticity index), and b^* (yellow-blue chromaticity index) in the CIELAB color space were obtained. The incident CIE (Commission Internationale de l'Eclairage) standard illuminant D65 and the observer of 10° were employed to calculate these colorimetric quantities. Luminous reflectance was taken into account for the color characterization. Chroma, C^*_{ab}, and hue angle, h_{ab}, for each sample were calculated using the following equations [9]:

$$C^*_{ab} = (a^{*^2} + b^{*^2})^{1/2} \quad (1)$$

$$h_{ab} = \tan^{-1}(b^*/a^*) \quad (2)$$

Three samples from each alloy were subjected to the above-described spectral reflectance and color coordinate measurements.

Optical microscopy

After carrying out the spectral reflectance measurement and color coordinate calculations, the samples were chemically etched in an aqua regia at room temperature and subjected to the microstructure examinations. Microstructures of the etched samples were observed using an optical microscope (Eclipse TE200, Nikon Corporation, Tokyo, Japan) under the bright-field illumination.

Electron probe microanalysis

Chemical compositions of each phase in the sample were analyzed by EPMA (electron probe microanalysis) according to the following methods. Plate samples with size 10 × 10 × 0.5 mm^3 annealed at 850 °C for 30 min in Ar gas stream were highly polished in the same manner as described in the preceding Subsect. "Spectrophotometric colorimetry". The polished plate samples were removed from the epoxy resin and set in an electron probe microanalyzer (JXA-8621 MX, JEOL Ltd., Tokyo, Japan). The analyzer was operated at an accelerating voltage of 20 kV and a probe current of 18 nA. Chemical compositions of the phases in the samples were determined by using the point analysis method. That is, intensities of AgLα, AuLα, PtLα, and CuKα characteristic X-rays from the target phases were recorded and the measurements were repeated five times at different positions in the sample. Chemical compositions of the target phases were determined by averaging the readings of the five measurements.

Results

Spectral reflectance curves

Figures 1, 2, and 3 show the spectral reflectance curves for the alloys containing 10, 15, and 20 at.% Cu, respectively. The geometry of diffuse illumination and 8° viewing was employed in the current spectral reflectance measurements. In each figure, spectral reflectance curves for three alloys with different Au concentrations are presented. It is seen that reflectance in the long wavelengths was high and was not affected greatly by Au concentration in each alloy group. With decreasing wavelength, reflectance gradually decreased and fairly dropped steeply in the short wavelength range in the visible spectrum. It is noted that in all three alloy groups, the steep part of the spectral reflectance

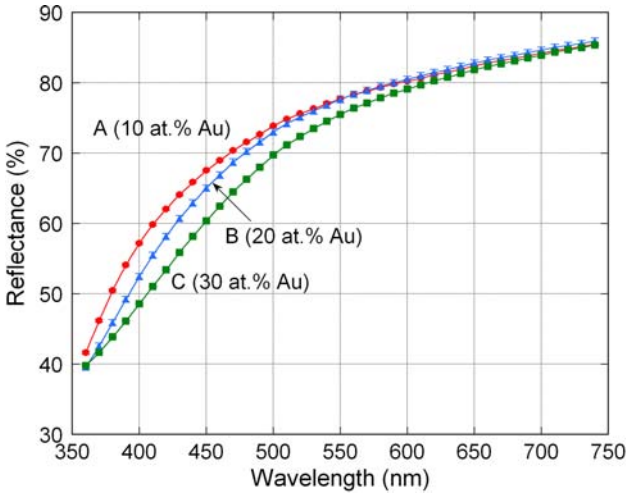

Fig. 1 Spectral reflectance curves for the Ag–Au–Pt–Cu alloys containing 10 at.% Cu

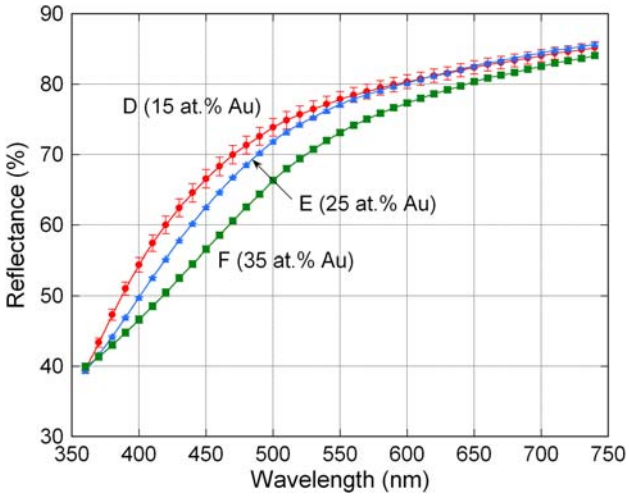

Fig. 2 Spectral reflectance curves for the Ag–Au–Pt–Cu alloys containing 15 at.% Cu

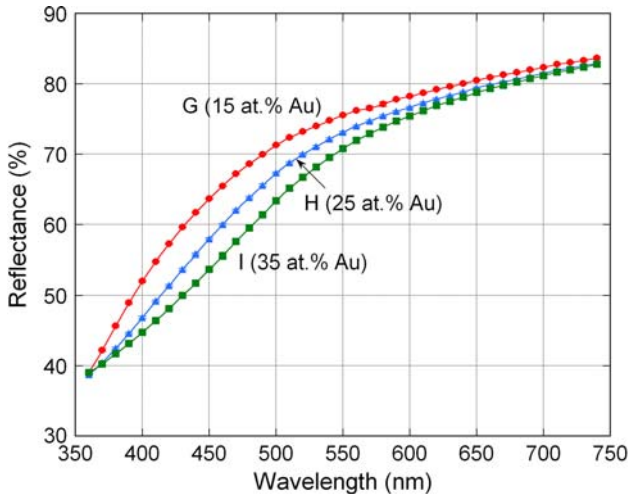

Fig. 3 Spectral reflectance curves for the Ag–Au–Pt–Cu alloys containing 20 at.% Cu

curve moved toward longer wavelengths with increasing Au concentration.

Color coordinates

Figure 4 shows distribution of chromaticity indices, a^* and b^*, in the three-dimensional CIELAB color space for all the alloys examined. Chromaticity indices for the component pure metals Ag, Au, Pt, and Cu were also presented for comparison. The a^* coordinate for the alloys ranged from −0.4 to 1.0 and did not vary greatly, showing the weak composition dependence of this parameter. On the other hand, the b^* coordinate appreciably varied from 8.0 to 14.4 depending on chemical composition, although these

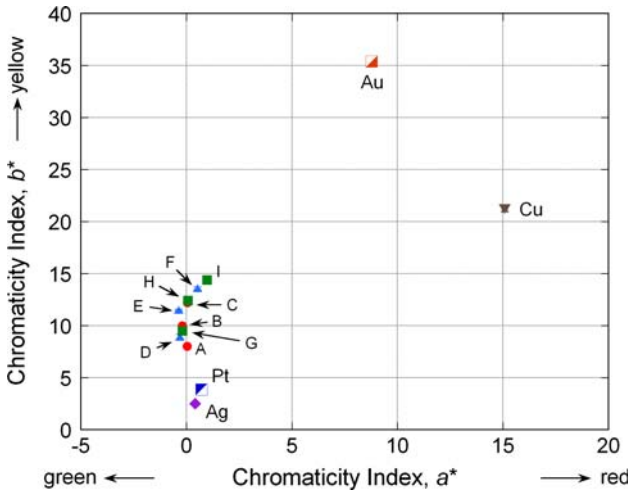

Fig. 4 Distribution of chromaticity indices, a^* and b^*, for all the experimental alloys and component pure metals Ag, Au, Pt, and Cu. The *circles* (A, B, and C), *triangles* (D, E, and F), and *squares* (G, H, and I) indicate the chromaticity indices for the alloys containing 10, 15, and 20 at.% Cu, respectively

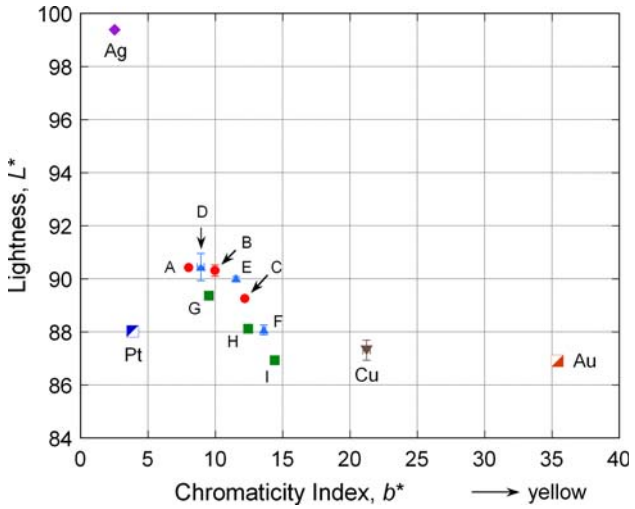

Fig. 5 Lightness, L^*_{ab} versus chromaticity index, b^*, plots for all the experimental alloys and component pure metals Ag, Au, Pt, and Cu

numbers were much lower than that for pure Au. It is noted that the alloy "A" with the lowest Au concentration showed the lowest b^* coordinate and the alloys "I" and "F" with the highest Au concentration showed high b^* coordinates.

Figure 5 shows distribution of lightness, L^*_{ab}, and yellow-blue chromaticity index, b^*, for all the experimental alloys and the component pure metals Ag, Au, Pt, and Cu. It is seen that the L^*_{ab} value for the experimental alloys ranged from about 90.4 for the alloys "A", "B", and "D" with high Ag concentrations to 86.9 for the alloy "I" with the lowest Ag concentration. In each of the three groups with the same Cu concentrations, the L^*_{ab} value slightly decreased with decreasing Ag concentration.

Figure 6 shows the relationship between chroma, C^*_{ab}, and hue angle, h_{ab}, for all the alloys examined. The alloy

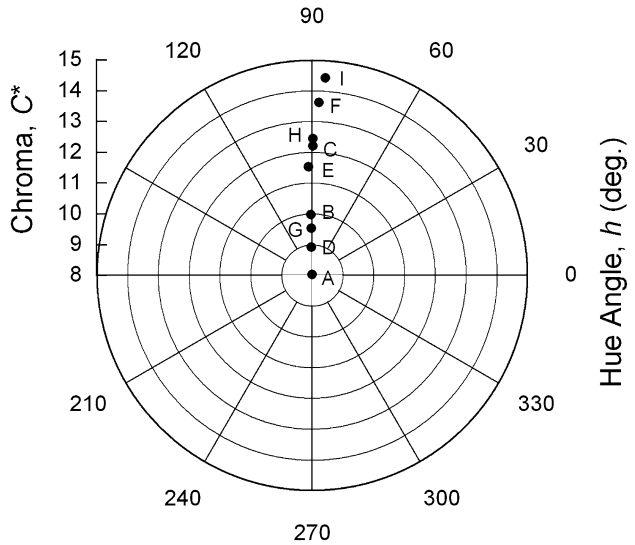

Fig. 6 Chroma, C^*_{ab} versus hue angle, h_{ab}, plots for all the experimental alloys

"A" with the highest Ag and the lowest Au concentrations showed the lowest chroma of 8.0, whereas the alloy "I" with the lowest Ag and the highest Au concentrations showed the highest chroma of 14.4. On the other hand, hue angles for most of the experimental alloys were distributed in a very narrow range near 90°. Only the alloy "I" with the lowest Ag and the highest Au and Cu concentrations showed a slightly lower hue angle.

It can be summarized that both the chroma, C^*_{ab}, and the yellow-blue chromaticity index, b^*, were substantially affected by chemical composition and that the yellowness substantially increased with increasing Au concentration in this series of alloys. Considering the facts that all the alloys contain some amount of Au and fall into the category of low-gold dental casting alloys, a pale yellow color is expected and preferable. The observed chromaticity indices, a^* and b^*, for all the alloys shown in Fig. 4 indicate that these alloys have a pale yellow color.

Microstructures and chemical compositions of the component phases

Optical microscopic observations showed that all the present Ag–Au–Pt–Cu alloys were a mixture of a major phase of the matrix and a minor phase of the small grains embedded in the matrix. Typical microstructures of the chemically etched alloys "C" containing 10 at.% Cu and "I" containing 20 at.% Cu are presented in Fig. 7a and b, respectively. It is clearly shown that the matrix only was attacked by the chemical etchant. The second-phase small grains were highly corrosion-resistant and accordingly observed with pure white contrast. It is noted that the second-phase grains were as small as 10 μm or less and that their highly corrosion-resistant nature was commonly recognized in all the alloys examined.

Table 3 gives the typical chemical compositions of the matrix and the second-phase small grains in the alloy "C" determined by the EPMA. The matrix was rich in Ag and Au, whereas the second-phase small grains were rich in Pt and Cu. The high corrosion-resistant nature of the second-phase grains shown in Fig. 7a and b is considered to be attributed to their high Pt and low Ag concentrations.

Crystal structures of the matrix and the second-phase small grains were not identified experimentally in the present study. However, their crystal structures can be reasonably speculated by referring the established phase diagrams. As given in Table 3, the EPMA study revealed that the matrix was rich in Ag and Au with small amounts of Pt and Cu and that the second-phase small grains were rich in Pt and Cu with small amounts of Au and Ag. Since all the alloys were well annealed at 850 °C and quenched into ice brine, phase equilibria at 850 °C may be concerned. According to the Ag–Au phase diagram [10], a continuous solid solution with the disordered face-centered-cubic (FCC) structure is formed at temperatures below the solidus line in the whole range of composition. Further, the Ag–Au–Pt [11] and Ag–Au–Cu [12] ternary phase diagrams show that the observed amounts of Pt and Cu in the matrix are soluble in the parent Ag–Au phase at 850 °C. Therefore, crystal structure of the Ag–Au-rich matrix phase is considered to be the disordered FCC structure.

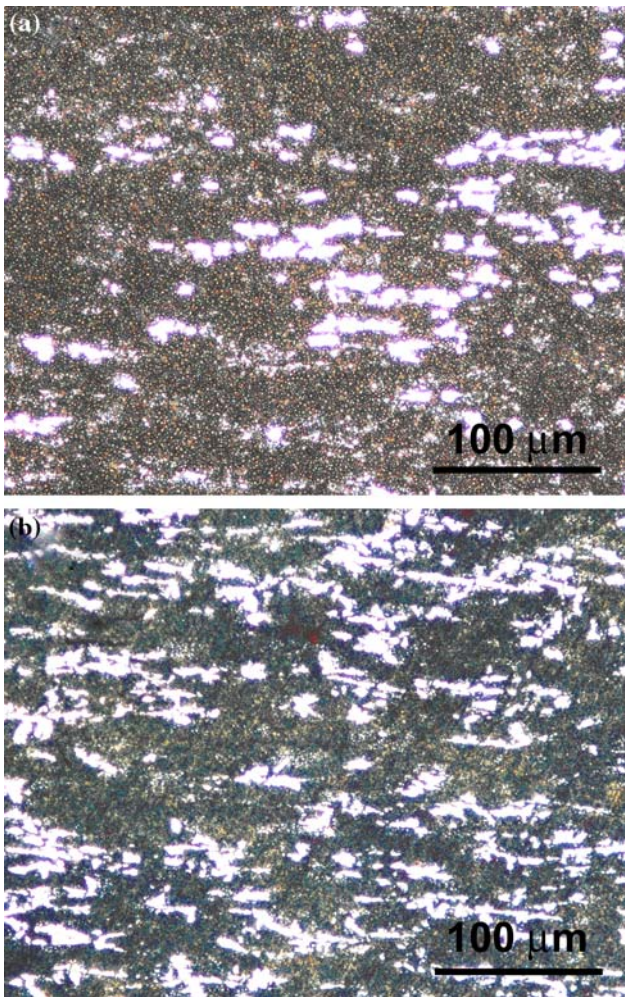

Fig. 7 Optical micrographs of the alloys "C" containing 10 at.% Cu (**a**) and "I" containing 20 at.% Cu (**b**), showing a two-phase microstructure consisting of the matrix (*dark contrast*) and the highly corrosion-resistant small grains (*white contrast*)

Similarly, the Cu–Pt phase diagram [13] shows that a continuous solid solution with the disordered FCC structure is stable at 850 °C in the whole range of composition. In addition to this complete solubility of Cu and Pt, the Ag–Pt [14] and Ag–Cu [15] phase diagrams suggest that the observed small amount of Ag is soluble in the parent Pt–Cu phase at 850 °C. With regard to the solubility of Au in the Pt–Cu phase, the Au–Cu phase diagram [16] shows that a continuous solid solution is stable at 850 °C in the whole range of composition. Based on the above-mentioned complete solubility of Pt and

Table 3 Chemical compositions of the component phases in the alloy "C" determined by EPMA

Phase	Composition (at.%)				Remarks
	Ag	Au	Pt	Cu	
Matrix	51.9 (0.6)	32.8 (0.6)	7.6 (0.2)	7.7 (0.3)	(Ag, Au)-rich
Second-phase small grains	3.7 (0.3)	8.4 (0.5)	44.1 (0.5)	43.8 (0.4)	(Pt, Cu)-rich

Numbers in parentheses indicate standard deviations for five measurements

Cu and that of Au and Cu, the Au–Pt phase diagram [17] suggests that the observed amount of Au is dissolved in the parent Pt–Cu phase at 850 °C. Accordingly, it may be reasonable to consider that crystal structure of the Pt–Cu-rich second-phase small grains is the disordered FCC structure.

Discussion

In general, various properties of metals and multi-phase alloys are known to be closely related to their microstructures, existent phases, and chemical compositions of each component phase [18, 19]. The present Ag–Au–Pt–Cu alloys annealed at 850 °C were with a two-phase microstructure consisting of the major phase of the Ag–Au-rich matrix and the minor phase of the Pt–Cu-rich small grains with size 10 μm or less distributed in the matrix. Accordingly, it may be reasonable to consider that the observed reflectance curves and the calculated color coordinates for the Ag–Au–Pt–Cu quaternary alloys can be interpreted on the basis of the reflectance and colorimetric quantities of each component phase. As presented in Table 3, the composition of the Pt–Cu-rich small grains was close to an equiatomic PtCu containing small amounts of Au and Ag. Further, the volume fraction of this second-phase was small in all the quaternary alloys examined. On the other hand, the Au/Ag atomic percentage ratios of the alloys were widely varied from 0.130 to 0.996 as given in Table 1. Therefore, to understand the optical properties of the quaternary Ag–Au–Pt–Cu alloys, we prepared an equiatomic PtCu alloy and binary Ag–Au alloys with various compositions as simplified models of the second-phase small grains and the matrix phase, respectively, and examined their optical properties in a similar manner. In the following subsections, we will discuss the optical properties of the quaternary Ag–Au–Pt–Cu alloys based on the observations of spectral reflectance curves and color coordinates for both the equiatomic PtCu and the series of Ag–Au alloys.

Optical properties of an equiatomic PtCu alloy

Figure 8 shows spectral reflectance curves for the equiatomic PtCu alloy and its component pure metals Cu and Pt. For pure Cu, reflectance in the long wavelength range

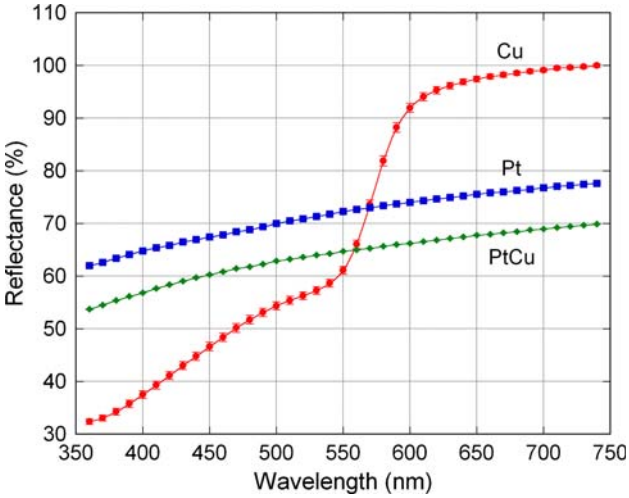

Fig. 8 Spectral reflectance curves for the equiatomic PtCu alloy and its component pure metals Pt and Cu

was very high, whereas reflectance in the short wavelength range was very low. As a result, a pronounced step in the spectral reflectance curve was observed near 570 nm. This observation of very high reflectance in the long wavelength range in the visible spectrum for pure Cu coincides well with the previous reports [20, 21]. The pronounced step in the spectral reflectance curve caused a red-orange appearance of Cu, as demonstrated in Fig. 9 in which the

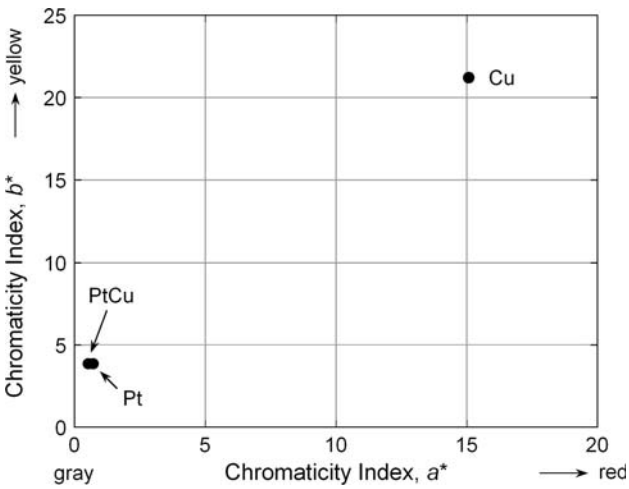

Fig. 9 Distribution of chromaticity indices, a^* and b^*, for the equiatomic PtCu alloy and its component pure metals Pt and Cu

observed chromaticity indices, a^* and b^*, for the equiatomic PtCu and its component pure metals are presented. For pure Pt, on the other hand, spectral reflectance was as low as 78% at 740 nm and the spectral reflectance curve was fairly flat throughout the whole range of visible spectrum, as seen in Fig. 8. This substantially low reflectance nature throughout the whole range visible spectrum is derived from the fact that the absorption of light for this transition metal begins in the infrared range, i.e., low energy range. Mott and Jones [22] suggested that in the transition metals Ni, Pd, and Pt, the work required to remove an electron from a state in the *d*-band to an empty state in the *s*-band is very small and the absorption of light in the infrared range may be due to such transition.

By alloying Cu with 50 at.% Pt, reflectance in the long wavelengths markedly decreased down to 70% at 740 nm and its spectral reflectance curve in the whole range of the visible spectrum was very similar to that for pure Pt, as seen in Fig. 8. Consequently, the observed chromaticity indices, a^* and b^*, for the equiatomic PtCu alloy were almost the same as those for pure Pt, as shown in Fig. 9. Since the a^* value for the PtCu alloy was 0.5 and the b^* value was as small as 3.9, the PtCu alloy was found to be almost colorless like pure Pt. These findings show that the alloying addition of Pt to Cu effectively decolorizes the Pt–Cu binary alloy and this strong decolorizing effect of Pt addition was caused by the pronounced flattening of the spectral reflectance curve in the visible spectrum. The above-described color characteristics of the PtCu alloy strongly suggest that the Pt–Cu-rich small grains in the Ag–Au–Pt–Cu alloys may be with low chroma. Further, the volume fraction of the Pt–Cu-rich small grains was small, as presented in Fig. 7. Consequently, it may be reasonable to consider that the contribution of the Pt–Cu-rich phase to the color of the quaternary Ag–Au–Pt–Cu alloys is very weak.

Optical properties of the Ag–Au binary alloys

As discussed above, the color of the quaternary Ag–Au–Pt–Cu alloys is considered to be primarily governed by the major phase of Ag–Au-rich matrix phase. To confirm this, we examined the optical properties of a series of Ag–Au binary alloys in the same manner.

Figure 10 shows the spectral reflectance curves for a series of binary Ag–Au alloys with 10, 20, 30, 40, and 50 at.% Au concentrations. Spectral reflectance curves for the component pure metals Ag and Au are also presented for comparison. For all the binary Ag–Au alloys, reflectance in the long wavelengths was very high, whereas it steeply dropped in the short wavelengths in the visible spectrum. It is clearly seen that the steep part of the spectral reflectance curve systematically moved toward the longer wavelengths in the visible spectrum with increasing Au

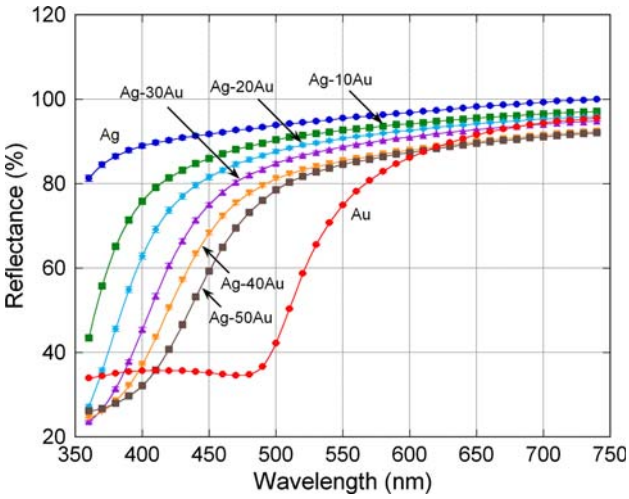

Fig. 10 Spectral reflectance curves for the binary Ag–Au alloys containing 10, 20, 30, 40, and 50 at.% Au and for their component pure metals Ag and Au

concentrations. Further, it is noted that reflectance in the long wavelength range slightly decreased with increasing Au concentration.

The fact that the alloying addition of Au to Ag continuously shifts the absorption edge of the spectral reflectance curve toward the longer wavelengths was previously reported by a few researchers [21, 23–25]. Since the electronic structure of Ag is very similar to that of Au, the effect of Au addition on color of Ag–Au binary alloys has been interpreted that the alloying addition of Au to Ag continuously raises the energy level of *d*-band [26]. Hence, the energy gap between the *d*-band and the Fermi level located above the *d*-band, which is decisive for the band transitions that govern the color, continuously decreases with increasing Au concentration [26]. As a result, the energy required for transition of *d*-electrons from the *d*-band to energetically higher Fermi level continuously decreases with increasing Au concentration.

Factors affecting the optical properties of the Ag–Au–Pt–Cu quaternary alloys

In the quaternary Ag–Au–Pt–Cu alloys, the absorption edge of the spectral reflectance curve moved toward longer wavelengths with increasing Au concentration as shown in Figs. 1, 2, and 3. This behavior agrees well with that for the binary Ag–Au alloys, as shown in Fig. 10. These results imply that the Au/Ag atomic ratio in an alloy may greatly affect the optical properties of both the quaternary Ag–Au–Pt–Cu and the binary Ag–Au alloys. To extract the controlling factors of the color of the present Ag–Au–Pt–Cu alloys, we analyzed the observed spectral reflectance curves for the quaternary Ag–Au–Pt–Cu and the binary Ag–Au alloys in terms of the positions of the absorption

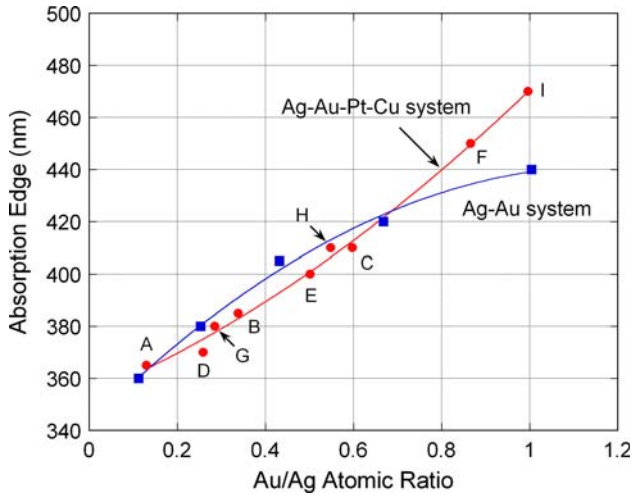

Fig. 11 Variations of absorption edge with Au/Ag atomic ratio for the quaternary Ag–Au–Pt–Cu (*circles*) and the binary Ag–Au (*squares*) alloys

edges of the spectral reflectance curves. Figure 11 shows variations of the absorption edges of the spectral reflectance curves with Au/Ag atomic ratio for both alloy systems. It can be seen that the absorption edge of the spectral reflectance curve systematically moved toward longer wavelengths in both systems and that both regression curves almost coincide with each other with only a slight deviation in the high Au/Ag atomic ratio range. This finding supports the validity of the above described consideration that the optical properties of the quaternary Ag–Au–Pt–Cu alloys are mainly governed by those of the major phase of the Ag–Au-rich matrix and that a controlling factor of color of the quaternary alloys is the Au/Ag atomic ratio.

Since the Au/Ag atomic ratio was found to be the primary controlling factor of the optical properties of the present Ag–Au–Pt–Cu alloys, the observed color coordinates in the CIELAB uniform color space were plotted against the Au/Ag atomic ratio in Fig. 12. The lightness L^*_{ab} slightly decreased from 90.4 to 86.9 with increasing Au/Ag atomic ratio from 0.130 to 0.996. This slight decrease in lightness is primarily caused by the slight decrease in total reflectivity in the whole range visible spectrum as shown in Figs. 1, 2, 3, and 10. The yellow-blue chromaticity index b^* substantially increased from 8.0 to 14.4, whereas the red-green chromaticity index a^* did not vary significantly. Figure 13 shows variations of chroma, C^*_{ab}, with Au/Ag atomic ratio for all the Ag–Au–Pt–Cu alloys. It is clearly shown that the chroma of an alloy systematically increased from 8.0 to 14.4 with increasing Au/Ag atomic ratio. Since the chroma C^*_{ab} is obtained according to the Eq. 1, this systematic increase in C^*_{ab} was found to be mainly caused by the systematic increase in b^* value with Au/Ag atomic ratio, as presented in Fig. 12.

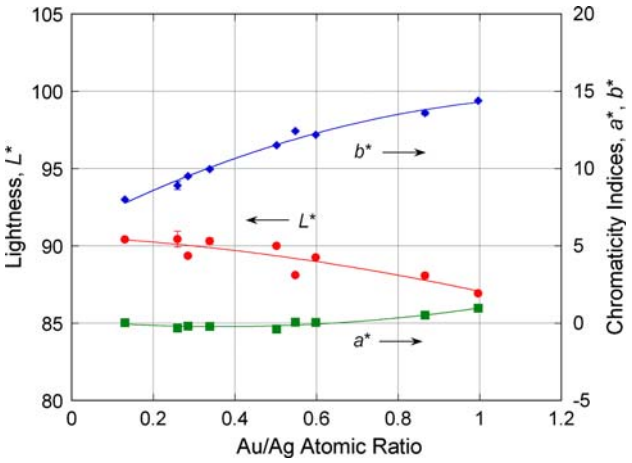

Fig. 12 Variations of lightness, L^*_{ab}, and chromaticity indices, a^* and b^*, with Au/Ag atomic ratio for the quaternary Ag–Au–Pt–Cu alloys

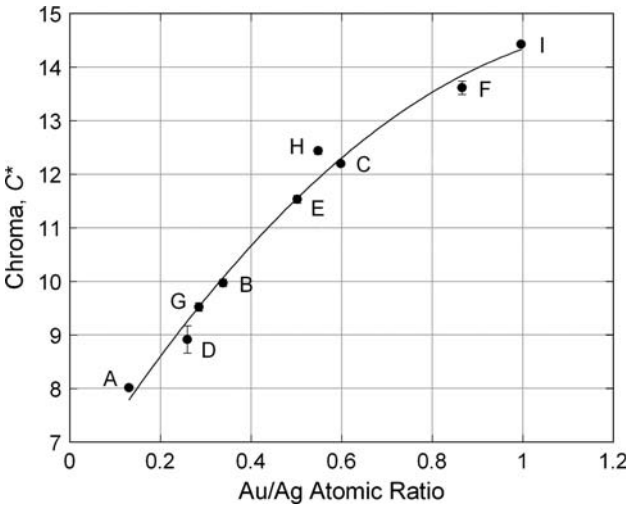

Fig. 13 Variations of chroma, C^*_{ab}, with Au/Ag atomic ratio for the quaternary Ag–Au–Pt–Cu alloys

We are carrying out biocompatibility evaluation by cell culture test, corrosion, and tarnish resistance evaluations for all the current alloys. Results of these studies show that all the alloys possess favorable characters as dental alloys. The results of a series of these studies will be published elsewhere.

Conclusions

Optical properties and microstructures of nine experimental Pd-free Ag–Au–Pt–Cu dental alloys containing 10 at.% Pt and 10–35 at.% Au were investigated in terms of spectral reflectance curves and structural analysis. The following conclusions were drawn.

1. All the Ag–Au–Pt–Cu alloys annealed at 850 °C were composed of a major phase of the Ag–Au-rich matrix

and a minor phase of the Pt–Cu-rich small grains embedded in the matrix.

2. The Pt–Cu-rich small grain phase was considered to be almost colorless, and accordingly the observed color of the quaternary Ag–Au–Pt–Cu alloys was substantially governed by the major phase of the Ag–Au-rich matrix phase.
3. Three-dimensional color coordinates, i.e., L^*_{ab} (lightness), a^* (red-green chromaticity index), and b^* (yellow-blue chromaticity index), in the CIELAB uniform color space for the Ag–Au–Pt–Cu alloys systematically varied as a function of Au/Ag atomic ratio in an alloy. That is, with increasing Au/Ag atomic ratio from 0.130 to 0.996, the L^*_{ab} value slightly decreased from 90.4 to 86.9 and the b^* value substantially increased from 8.0 to 14.4. On the other hand, the a^* value did not vary significantly.
4. Chroma, C^*_{ab}, systematically increased from 8.0 to 14.4 with increasing Au/Ag atomic ratio from 0.130 to 0.996. This variation of chroma was primarily caused by the systematic increase in the b^* value.

Acknowledgements This research was supported in part by "The Grant-in-Aid for Scientific Research" from The Ministry of Education, Culture, Sports, Science and Technology in Japan (13672044). The authors also thank Mr. Y. Murakami of The Institute of Metals Research, Tohoku University (Sendai, Japan) for his assistance in electron probe microanalysis.

References

1. Phillips RW (1991) Skinner's science of dental materials, 9th edn. WB Saunders Company, Philadelphia, p 359
2. Kendall T (2004) Platinum 2004. Johnson Matthey, London, England, p 8
3. Kendall T (2004) Platinum 2004. Johnson Matthey, London, England, p 54
4. Kendall T (2005) Platinum 2005. Johnson Matthey, London, England, p 36
5. Jollie D (2007) Platinum 2007. Johnson Matthey, Royston, England, p 4
6. Wataha JC, Hanks CT (1996) J Oral Rehabil 23:309
7. Knosp H, Holliday RJ, Corti CW (2003) Gold Bull 36(3):93
8. German RM, Guzowski MM, Wright DC (1980) J Metals 32:20
9. CIE Technical Report (2004) Colorimetry, vol 15, 3rd edn. CIE Central Bureau, Vienna
10. Massalski TB (1990) Binary alloy phase diagrams, vol 1, 2nd edn. ASM International, Materials Park, Ohio, USA, p 12
11. Prince A, Raynor GV, Evans DS (1990) Phase diagrams of ternary gold alloys. The Institute of Metals, London, UK, p 60
12. Prince A, Raynor GV, Evans DS (1990) Phase diagrams of ternary gold alloys. The Institute of Metals, London, UK, p 7
13. Massalski TB (1990) Binary alloy phase diagrams, vol 2, 2nd edn. ASM International, Materials Park, Ohio, USA, p 1460
14. Massalski TB (1990) Binary alloy phase diagrams, vol 1, 2nd edn. ASM International, Materials Park, Ohio, USA, p 77
15. Massalski TB (1990) Binary alloy phase diagrams, vol 1, 2nd edn. ASM International, Materials Park, Ohio, USA, p 28
16. Massalski TB (1990) Binary alloy phase diagrams, vol 1, 2nd edn. ASM International, Materials Park, Ohio, USA, p 358
17. Massalski TB (1990) Binary alloy phase diagrams, vol 1, 2nd edn. ASM International, Materials Park, Ohio, USA, p 414
18. Cheng F, Nishikawa H, Takemoto T (2008) J Mater Sci 43:3643. doi:10.1007/s10853-008-2580-7
19. Yung KC, Wu SP, Liem H (2009) J Mater Sci 44:154. doi:10.1007/s10853-008-3119-7
20. Biondi MA, Rayne JA (1959) Phys Rev 115:1522
21. Roberts EFI, Clarke KMC, Hunt R (1980) Mater Sci Eng 42:71
22. Mott NF, Jones H (1958) The theory of the properties of metals and alloys. Dover Publications, Inc., New York, p 119
23. Wessel PR (1963) Phys Rev 132(5):2062
24. Fukutani H, Sueoka O (1966) In: Abelès F (ed) Optical properties and electronic structure of metals and alloys. North-Holland Publishing Company, Amsterdam, The Netherlands, p 565
25. Roberts EFI, Clarke KM (1979) Gold Bull 12:9
26. Saeger KE, Rodies J (1977) Gold Bull 10:10